

LEGO: Learning and Graph-Optimized Modular Tracker for Online Multi-Object Tracking with Point Clouds

Zhenrong Zhang*, Jianan Liu*, Yuxuan Xia, Tao Huang, *Senior Member, IEEE*,
 Qing-Long Han, *Fellow, IEEE*, and Hongbin Liu†, *Member, IEEE*

Abstract—Online multi-object tracking (MOT) plays a pivotal role in autonomous systems. The state-of-the-art approaches usually employ a tracking-by-detection method, and data association plays a critical role. This paper proposes a learning and graph-optimized (LEGO) modular tracker to improve data association performance in the existing literature. The proposed LEGO tracker integrates graph optimization and self-attention mechanisms, which efficiently formulate the association score map, facilitating the accurate and efficient matching of objects across time frames. To further enhance the state update process, the Kalman filter is added to ensure consistent tracking by incorporating temporal coherence in the object states. Our proposed method utilizing LiDAR alone has shown exceptional performance compared to other online tracking approaches, including LiDAR-based and LiDAR-camera fusion-based methods. LEGO ranked 1st at the time of submitting results to KITTI object tracking evaluation ranking board and remains 2nd at the time of submitting this paper, among all online trackers in the KITTI MOT benchmark for cars¹.

Index Terms—Multi-object tracking, online tracking, transformer, graph optimization, graph neural network, data association, track management, LiDAR, point cloud, autonomous driving

I. INTRODUCTION

MULTI-OBJECT tracking (MOT) is a crucial technology utilized in various systems within the field of intelligent transportation systems (ITS), including advanced driver assistance systems (ADAS) and autonomous driving (AD). Fig. 1 illustrates the task of LiDAR-based MOT, which presents several challenges that need to be addressed:

- Refinement of state information: The tracker should refine the state information provided by preceding modules, such as instance segmentation [1][2] and object detection

This work has been submitted to the IEEE for possible publication. Copyright may be transferred without notice, after which this version may no longer be accessible.

*Both authors contribute equally to the work and are co-first authors.

†Corresponding author.

Z. Zhang and H. Liu are with the School of AI and Advanced Computing, Xi'an Jiaotong-Liverpool University, Suzhou, P.R. China. Email: Zhenrong.Zhang21@student.xjtu.edu.cn; Hongbin.Liu@xjtu.edu.cn.

J. Liu is with Vitalent Consulting, Gothenburg, Sweden. Email: jianan.liu@vitalent.se.

Y. Xia is with Department of Electrical Engineering, Chalmers University of Technology, Gothenburg 41296, Sweden. Email: yuxuan.xia@chalmers.se.

T. Huang is with College of Science and Engineering, James Cook University, Cairns, QLD 4878, Australia. Email: tao.huang1@jcu.edu.au.

Q.-L. Han is with the School of Science, Computing and Engineering Technologies, Swinburne University of Technology, Melbourne, VIC 3122, Australia. Email: qhan@swin.edu.au.

¹https://www.cvlabs.net/datasets/kitti/eval_tracking.php

[3][4][5]. By incorporating this refined state information, the tracker contributes to the overall accuracy and efficacy of the tracking system.

- False detection rejection: To enhance the overall reliability of the tracking process, it is essential for the tracker to possess the capability to discern and disregard inaccurate detections produced by the object detector. This ability to filter out false positives is crucial for maintaining accurate tracking results.
- Identification (ID) estimation and tracking continuity: Another significant challenge in multi-object tracking is maintaining tracking continuity even in situations where the object fails to be detected across successive frames. The tracker should be able to handle occlusions, temporary disappearances, or other situations that can interrupt object detection, ensuring robust and uninterrupted monitoring of the objects. This entails assigning and preserving a unique identification marker for each object, ensuring its continuity and consistency.

Effectively addressing the challenges in MOT is paramount for developing robust and accurate tracking systems. The existing MOT methods can be categorized into distinct groups based on the sensor modalities they utilize. These categories encompass 2D MOT methods, 3D MOT techniques relying solely on LiDAR sensors, and 3D MOT methods that leverage both camera and LiDAR systems. In the realm of 2D MOT, notable methods, such as FairMOT [6], ByteTrack [7], and StrongSort [8] predominantly employ camera data for tracking objects. Although these methods provide valuable insights, their performance is constrained by the limitations of working with 2D representations alone. On the other hand, 3D MOT techniques exclusively employ LiDAR sensors to capture 3D information about the tracked objects. AB3DMOT [15] serves as an exemplary method within this category, demonstrating the efficacy of LiDAR-based approaches for precise object localization and spatial understanding. Furthermore, there exist 3D MOT methods that capitalize on the synergies between camera and LiDAR systems. Probabilistic CBMOT [41] represents one such approach, where both sensor modalities are utilized to improve tracking performance. By combining the strengths of cameras and LiDAR sensors, these methods aim to achieve enhanced object tracking accuracy. A majority of these MOT methods can be classified as tracking-by-detection methods, wherein 3D detectors play a central role. Various 3D detectors have been developed to facilitate object detection in



Fig. 1: Illustration of a MOT method via detection utilizing LiDAR for ADAS and AD: This figure delineates the tracking result at two successive time frames $t - 1$ and t , shown in birds eye's view (BEV), the different colours show different tracked objects.

the MOT pipeline. Examples include PointRCNN [9], PointGNN [10], CenterPoint [11], and CasA [12], among others. In this research, the tracking-by-detection task for MOT with a specific focus on utilizing LiDAR is adopted. The proposed approach consists of a two-stage process, which involves an initial object detection step followed by a subsequent tracking phase. During the object detection stage, the detector analyzes the input frames and generates relevant information, such as bounding box dimensions and object centre location in 3D. These outputs provide valuable cues about the location and extent of the detected objects within the 3D space. Following the object detection stage, the tracking phase is employed to refine and synthesize the acquired data. In this phase, a tracking algorithm is applied to associate and maintain the IDs of the objects across different frames. Specifically, the tracker assigns unique track IDs to each bounding box, enabling consistent identification of objects throughout the tracking process.

The tracking phase is initiated by generating pairwise affinities, which play a crucial role in associating objects across time frames. Various methods have been employed to compute these affinities in the context of MOT, including feature representation techniques, such as appearance similarity, distance metrics, and motion predictions. In recent years, deep learning-based features rooted in convolutional neural networks (CNN) [37] have gained widespread adoption for computing these affinities. Additionally, a multi-cue approach [55] which incorporates motion as an additional cue, has been adopted to complement appearance features for data association. While motion modules based on deep learning, such as long short-term memory (LSTM) [56], have shown limited robustness and efficiency when compared to motion prediction methods using the Kalman filter [16], relying solely on intersection over union (IoU) and Kalman filter introduces certain challenges. Firstly, there is a loss of point cloud information, and secondly, geometric similarity computed solely based on IoU lacks reliability. Although some studies have employed deep learning-based methods, such as [19], to derive the cost matrix, the noise-corrupted output from the detector limits the feature learning capabilities of deep neural networks. Moreover, the trajectory representation, which consists of a topology unsuited for CNN or recurrent neural networks (RNN), poses challenges when dealing with unstructured data. Considering the trajectory as an edge comprising multiple object nodes suggests that

a graph neural network (GNN) can be a suitable deep learning model for this task. However, the direct application of GNN presents certain issues, including the compromised calculation efficiency due to the high dimensionality of the graph and the information redundancy caused by uniform message passing from neighboring nodes [60].

To tackle the aforementioned challenges, an appealing approach is by redefining the data association problem as a bipartite graph matching problem, which takes advantage of its graphical formulation. In this redefined context, a self-attention-based GNN is integrated with the Kalman filter to facilitate data association and perform state updates.

Our approach incorporates a self-attention-based GNN optimization module, which operates by reasoning over non-Euclidean graph data through message passing. This module enhances the relational reasoning abilities of the system and reduces information redundancy. By leveraging self-attention mechanisms, our GNN can effectively capture long-range dependencies and complex relationships between objects, contributing to improved data association accuracy. Additionally, an offset module is specifically designed to refine the estimated bounding boxes from the detector. The primary objective of this module is to correct the output of the detector, resulting in more accurate and reliable information about the object's motion.

The contributions of this paper are outlined as follows:

- A learning and graph-optimized (LEGO) modular tracker is proposed for online MOT. The tracker is built upon recent model-based tracker, i.e. PC3T [38], with introducing two additional learning modules, an offset correction module and a self-attention based GNN, which are easily comprehensible, tunable, and adaptable to different sensor modalities.
- The offset correction module is designed to predict the offset between these detection results and the ground truth. The primary purpose of this mechanism is to rectify prediction outcomes, thereby improving the accuracy of the model's predictive capabilities. The graph dual attention network (GDAN) is introduced to process the bipartite graph input to reduce the information redundancy, and directly generate the association score matrix.
- Empirical evaluation and performance analysis: The paper empirically evaluates the proposed GDAN module, demonstrating its effectiveness in enhancing tracking

performance. The proposed LEGO is evaluated using the KITTI MOT benchmark, and the results showcase commendable performance in terms of tracking accuracy and reliability.

The structure of this paper is organized as follows: Section II presents a thorough review of related works in the field of LiDAR-based MOT within the context of autonomous driving applications. Section III introduces the proposed LEGO Modular tracker, elucidating its key components and functionalities. Subsequently, in Section IV, the experimental results are presented and analyzed in detail. Finally, the paper concludes with Section V, summarizing the key findings and contributions of the study.

II. RELATED WORK

A. MOT with LiDAR Only

1) *Model-based Methods*: Similar to MOT tasks in image filed [13][14], contemporary tracking systems in ADAS and AD applications often employ global nearest neighbor methods and heuristics for data association. In LiDAR-based MOT, several methods have emerged that rely exclusively on LiDAR sensors. Chiu et al. [17] made a pioneering contribution by integrating Mahalanobis distance with AB3DMOT, establishing a benchmark for addressing LiDAR-based 3D MOT challenges. Similarly, SimpleTrack [22] introduced a generalized version of 3D IoU, known as GIoU, as the scoring mechanism for tracking-by-detection tasks. Bytetrackv2 [32] employed a hierarchical data association strategy to identify genuine objects within low-score detection boxes, effectively mitigating issues related to object loss and fragmented trajectories. Additionally, this system employed non-maximum suppression (NMS) to preprocess object detections. Empirical evidence demonstrated that combining GIoU with NMS preprocessing enhanced overall tracking performance.

Maintaining tracks even when objects are no longer visible is a common feature shared by ImmortalTracker [23] and PC3T [38]. This helps reduce identification switches and fragmented tracks. ACK3DMOT [33] introduced a cost matrix for tracking-by-detection tasks based on a joint probability function that considers appearance, geometry, and distance correlation between detected bounding boxes and predicted objects. When combined with an adaptive cubature Kalman filter, this approach achieved enhanced tracking performance. PF-MOT [26] utilized a cluster-based earth-mover distance, Euclidean distance, and feature similarity to construct the cost matrix. Considering uncertainties, UG3DMOT [36] evaluated data association based on random vectors, where the similarity between two multidimensional distributions was evaluated using the Jensen-Shannon divergence.

There are alternative algorithms where each potential object is modelled using a Bernoulli process with probabilistic object existence. RFS-M3 [18] utilized the Poisson multi-Bernoulli mixture filter based on a random finite set (RFS) to tackle the LiDAR-based MOT problem. Through systematic comparative analysis, GNN-PMB [28] demonstrated that the contemporary RFS-based Bayesian tracking framework outperformed the traditional random vector-based Bayesian tracking framework.

BP-Tracker [24] presented a factor graph formulation of the MOT problem and employed a belief propagation algorithm to compute the marginal association probability, representing a significant advancement in the field.

2) *Deep-learning based Methods*: SimTrack [19] and CenterTube [34] introduce end-to-end trainable models for joint detection and tracking, leveraging raw point cloud as input. OGR3MOT [20], Batch3DMOT [21], PolarMOT [35], Rethinking3DMOT propose sophisticated graph structures based on neural message passing, enabling online execution of detection and tracking processes. The ENBP-Tracker [27] integrates GNN into its design, distinguishing itself by combining the network with a belief propagation tracker. This hybrid tracking architecture enhances the robustness and efficacy of the tracking process, showcasing the potential of merging traditional tracking methods with advanced neural network architectures. Intertrack [29] TransMOT [25] adopt transformer structures to generate discriminative object representations for data association. Minkowski-Tracker [30], PC-TCNN [39], ShaSTA [31] employ proposal networks to extract features from various feature maps, facilitating the learning of affinity matrix for point cloud-based MOT.

B. MOT with LiDAR and Camera Fusion

The effectiveness of MOT can be further enhanced by adopting a fusion approach that combines data from LiDAR and camera sources. Several methods, such as Probabilistic3DMM [40], CBMOT, GNN3DMOT [43], and AlphaTrack [42] have utilized this fusion approach to leverage the complementary strengths of different sensor modalities, leading to more comprehensive and precise object tracking. IMSF MOT [44] proposes a novel feature fusion method using Pointnet++ to extract more discriminative features and improve multiple object tracking performance.

DeepFusionMOT [48] and EagerMOT [45] improve tracking performance compared to Probabilistic3DMM by implementing a two-stage data association scheme. This scheme leverages 3D detection data obtained from LiDAR and camera inputs, and 2D detection data obtained solely from the camera. By combining information from multiple modalities, a more comprehensive understanding of the environment is achieved, potentially enhancing the robustness and accuracy of the tracking process.

Building upon EagerMOT, AlphaTrack introduces a feature extractor that concatenates image and point cloud information as input to enhance performance. Additionally, other relevant works, such as DualTracker [47], HIDMOT [50], CAMO-MOT [52], MSA-MOT [51], and JMOT [46] utilize Point-GNN or PointRCNN as their 3D object detectors to estimate object detections. They are combined with detection proposals from image data, and a hybrid multi-modal input is employed for the association within the tracking-by-detection task, potentially improving the overall performance and accuracy of the tracking system.

III. THE PROPOSED LEGO MODULAR TRACKER

Within this section, we will introduce the LEGO modular tracker. Firstly, we will present its overall framework, followed

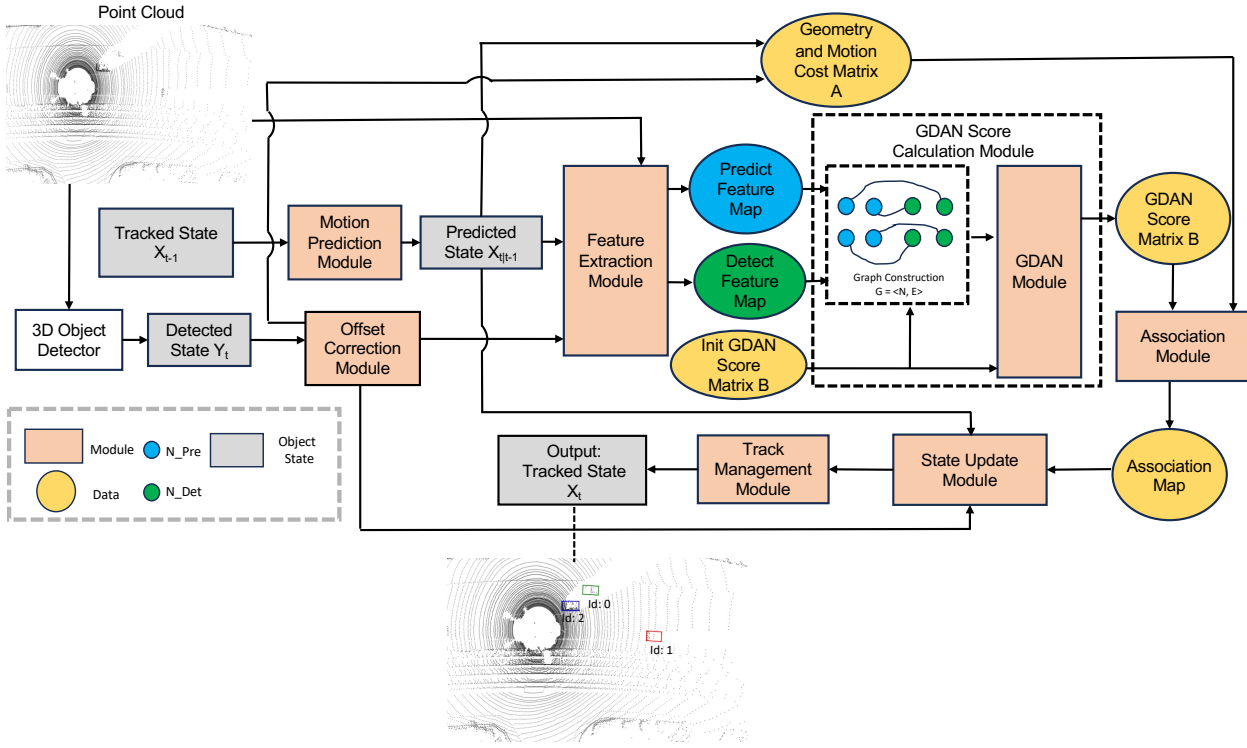


Fig. 2: The proposed LEGO tracker seamlessly integrates several modules. First, the offset correction module refines detection results and corrects detected errors. Simultaneously, the motion prediction module utilizes the tracked state X_t to forecast the next state $X_{t|t-1}$. The feature extraction module then derives 3D feature maps for both predicted and detected objects. Using this information, the GDAN score calculation module constructs a bipartite graph and computes the GDAN score matrix. The association module subsequently integrates the geometry and motion cost matrix with the GDAN score matrix, yielding an association map. Finally, the state update module refines the predicted state, and the track management module processes the matched detected states, completing the tracking cycle.

by a detailed elaboration of each module. Fig. 2 shows the proposed LEGO tracker, which comprises several modules: motion prediction, offset correction, feature extraction, GDAN score calculation, association, state update, and track management.

A. The Framework of LEGO Modular Tracker

Initiating the process, the 3D point cloud is fed into a 3D object detector, which is responsible for identifying potential objects within the scene. To augment the accuracy of the detection results, an offset correction module is proposed. The primary function of the offset correction module is to anticipate the offset between the detection result and the ground truth, thereby smoothing the detector's outputs. Meanwhile, the motion prediction module takes the tracked state from the previous timestep and predicts the state of each object in the current timestep by Kalman prediction. Then, the geometry and motion cost matrix A is calculated by the detected state (after the offset correction module) and the predicted state from the motion prediction module.

To extract the robust 3D point cloud features, the outputs of the previous motion prediction and offset correction modules along with the 3D point cloud are fed into the feature extraction module, which utilizes the PointNet architecture [58] to produce the feature maps. Sequentially, a bipartite graph $G = \langle N, E \rangle$ is constructed with the predicted feature map and

the detected feature map. Here, $N = (N_{det}, N_{pre})$ represents the set of nodes for detected objects and predicted objects and edges E represent the potential association between detected and predicted objects.

Upon inputting the bipartite graph G and the init GDAN score matrix into the GDAN module, the GDAN score matrix B is produced as an output. The final association cost matrix is then obtained via the proposed method, encapsulating both the GDAN score matrix and the geometry and motion cost matrix. The data association module is utilized to discern the matched pairs. Finally, the association map is fed into the state update module, prompting an update in the detected state within the aforementioned module being conveyed to the track management module.

B. Motion Prediction Module

Recently, LSTM networks have become increasingly popular in MOT methods for predicting changes in the object state [57]. These networks are favoured for their ability to handle sequential data exceptionally well. However, it is important to note that LSTM networks require more time than traditional motion prediction techniques, like those based on the Kalman filter. Certain MOT techniques prefer using a constant velocity motion model rather than LSTM networks. However, this model assumes that the object moves at a nearly constant speed, which may not hold true in several real-world situations.

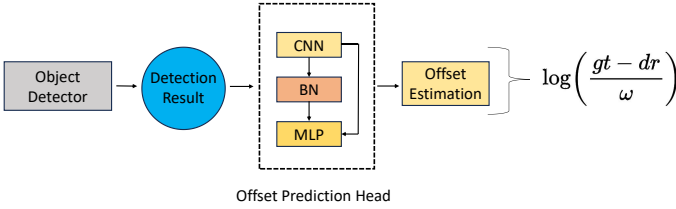


Fig. 3: The structure of the offset correction module. The detection result, which comprises parameters $x_p^d, y_p^d, z_p^d, w^d, h^d, l^d$, is inputted into the offset prediction head. The offset prediction head can be construed as a simple neural network, which computes the offset between the ground truth and the obtained detection result.

As a result, if there are consecutive missed detections, it could lead to considerable errors in motion prediction. To overcome this problem, the constant acceleration (CA) motion model [16] is used, which offers a more precise representation of the object state. In the CA motion model, the object state \mathbf{X}_{t-1} at a specific temporal instance $t-1$ is represented as $[\mathbf{pos}_{t-1}, \mathbf{v}_{t-1}, \boldsymbol{\alpha}_{t-1}]^T$, where \mathbf{pos}_{t-1} denotes the position, \mathbf{v}_{t-1} represents the velocity, and $\boldsymbol{\alpha}_{t-1}$ indicates the orientation of the object. The prediction of the mean state $\mathbf{X}_{t|t-1}$ and covariance $\mathbf{P}_{t|t-1}$ using Kalman prediction equations with the CA motion model is as follows:

$$\mathbf{X}_{t|t-1} = \mathbf{S}\mathbf{A}\mathbf{X}_{t-1}, \quad (1)$$

$$\mathbf{P}_{t|t-1} = \mathbf{S}\mathbf{A}\mathbf{P}_{t-1}\mathbf{A}^T + \mathbf{Q}, \quad (2)$$

where $\mathbf{S}\mathbf{A}$ is the state transition matrix, \mathbf{Q} represents the motion noise covariance matrix, \mathbf{I} denotes the identity matrix, \mathbf{O} represents the zero matrix, n denotes the state dimension, and δ and \mathbf{a} are sensor-related hyper-parameters.

C. Offset Correction Module

Our investigation has revealed a significant issue related to the accuracy of the state inferred by the detector, especially when errors arise from the 3D object detector. In order to mitigate this potential source of inaccuracies, the integration of an offset correction module is proposed. This module serves the crucial purpose of rectifying the detection outcomes generated by the 3D object detector, thereby enhancing the overall accuracy of the system. The architecture and components of this offset correction module are depicted in Fig. 3. This module comprises a 3D convolution layer, batch normalization layer, and multi-layer perception (MLP) with the residual connection. The offset obtained from the head is given by

$$O = \log\left(\frac{gt - dr}{\beta}\right), \quad (3)$$

where $gt = (x_p^g, y_p^g, z_p^g, w^g, h^g, l^g)$ represents the ground truth coordinates (x_p^g, y_p^g, z_p^g) , width w^g , height h^g , length l^g ; $dr = (x_p^d, y_p^d, z_p^d, w^d, h^d, l^d)$ indicates the object detection extracted from the 3D object detector, and β is the scaling factor. Through Eq. (3), the discrepancies of object detection are smoothed.

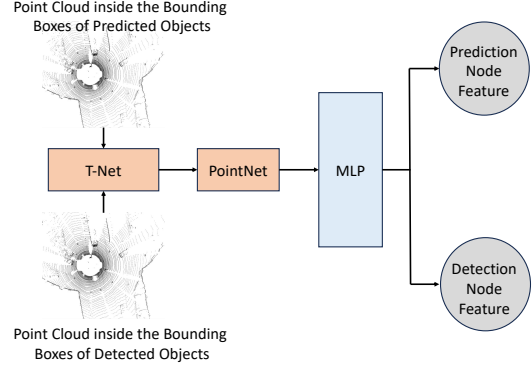


Fig. 4: The structure of the feature extraction module. The 3D point cloud is served as input into the transformation network (T-Net), where they undergo augmentation before being fed into the PointNet architecture. Following this, the outputs of the penultimate layer of the PointNet are channelled into the multi-layer perception (MLP). This subsequent step yields the desired outputs: the prediction node feature and the detection node feature.

D. Feature Extraction Module

The feature extraction module uses a combination of information from two important parts: the detected state after the offset correction module and the predicted state from the motion prediction module. This combination helps create feature maps that highlight important characteristics of the object being targeted, using data from the 3D point cloud within the bounding box.

1) *3D Point Cloud Feature Extractor*: To begin the process, the 3D point cloud is extracted from within the 3D bounding boxes using information from both the detected and predicted states. The extracted point cloud undergoes spatial adjustments using a transformation network (T-Net) before being passed through the PointNet architecture. The PointNet architecture plays a key role in generating a feature representation of the 3D point cloud data, resulting in a feature map denoted as $\mathbf{F}_{3d} = (f_{3d_1}, f_{3d_2}, f_{3d_3}, \dots, f_{3d_n})$. Each element in the feature map represents the feature vector of the object present within the 3D bounding boxes.

2) *Feature Embedding*: Sequentially, the 3D point cloud feature map is fed into the MLP-based embedding network, to extract embedded features as illustrated in Fig. 4. This process can be described as

$$\mathbf{F} = (MLP(\mathbf{F}_{3d})), \quad (4)$$

where \mathbf{F} denotes the output feature maps of the feature extraction module.

E. GDAN Score Calculation Module

Utilizing the feature map extracted from the feature extraction module, a GDAN score matrix, denoted as \mathbf{B} , is calculated through the GDAN score calculation module. Similar to [40], the purpose of employing such matrix is to extract the similarities between different detections and predicted tracks. This calculation takes into consideration the relationships between point cloud voxels of various objects. We first construct the graph. Most of the recent works which applied GNN for

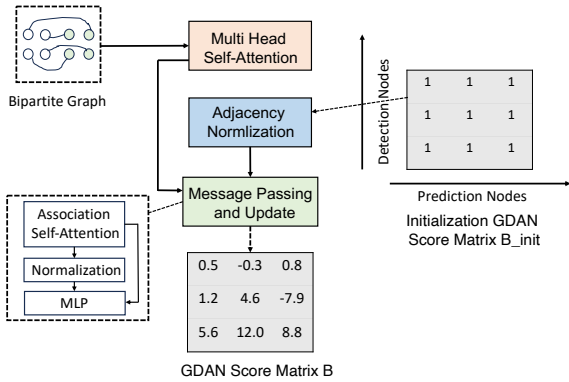


Fig. 5: The architecture of GDAN module. In the initial stage, a bipartite graph is fed into the multi-head self-attention (MSA) block. This data together with the normalized initialization GDAN association score matrix in the combined framework of message passing and update block. This block includes several components: an association self-attention mechanism that adjusts the original self-attention, a normalization layer, and an MLP. Finally, this comprehensive system yields the output in the form of an association score matrix.

3D MOT, e.g. PTP [53], Rethinking3DMOT [37], 3Dmotformer [54], etc, use the fully connected graph with dimension of $(J + U) \times (J + U)$. However, such graph entails redundant computations due to the simultaneous inclusion of detection and prediction nodes. To this end, we follow GNN3DMOT [43] to use the prior knowledge that the matching should only happen across frames that we construct a bipartite graph. The structure of the graph is represented as a matrix of dimensions $J \times U$, where J represents the number of detection nodes and U denotes the number of prediction nodes. The bipartite graph mitigate this computational redundancy, effectively reducing the dimension of the association score matrix to $J \times U$. Consequently, the association between predicted and detected objects is framed as a maximum-weighted bipartite matching problem, wherein each edge in the graph corresponds to an association score between two distinct nodes. Formally, the bipartite graph is represented as $\mathbf{G} = \langle \mathbf{N}, \mathbf{E} \rangle$, with \mathbf{N} consisting of two node sets, \mathbf{N}_{det} (the set of nodes representing detected objects) and \mathbf{N}_{pre} (the set of nodes representing predicted objects). The cardinalities of these sets are $|\mathbf{N}_{det}| = J$ and $|\mathbf{N}_{pre}| = U$, respectively. The set of edges, \mathbf{E} , captures the associations between nodes, and each edge within \mathbf{E} encodes an association score representing the strength of the relationship between the corresponding nodes. To initialize the bipartite graph, all edge values are assigned an initial score of 1.

Subsequently, the initial GDAN score matrix denoted as \mathbf{B}_{init} , in conjunction with the predicted feature map and detected feature map, serves as input parameters for further processing. This sequential computation culminates in the generation of a GDAN score matrix denoted as $\mathbf{B} \in \mathbb{R}^{J \times U}$, representing the importance of each pairwise similarity in the final scoring scheme.

The method in [59] directly applies polynomials to update the feature information on the node through message passing. This could result in redundant information for each node since

different nodes should contribute different useful information instead of having the same contribution for message passing. To overcome the limitations in [59], GNN3DMOT [43] use graph attention network (GAT) [60] to realize the message passing and updating. However, GAT belongs to the spatial convolution and process the message passing and updating node by node which ignoring the whole structure of the graph. This could miss the important information in the graph we construct. To overcome these limitations, we proposed the GDAN module. We first use an MSA encoder to simple extract the feature representation of each node. Considering the input are point cloud in two sequence frames, we also design an embedding network with LSTM and several fully connect layers to further extract the embedding representation of features, then a modified self-attention-based mechanism is incorporated to manage message passing and updating within the bipartite graph. Different from directly using self-attention like GAT, we add a learnable adjacency matrix into the calculation of the self-attention during the message passing and updating process which can provide the structure information. Our proposed modified self-attention blocks are specifically tailored to suit the bipartite graph structure, as depicted in Fig. 5.

The association self-attention calculation method undergoes modification to enable the learning of association scores via:

$$\text{Attention}(\mathbf{Q}, \mathbf{K}, \mathbf{V}, \mathbf{B}) = f(\mathbf{Q}, \mathbf{K}, \mathbf{V}) \times \mathbf{W} \times \mathbf{B}^T, \quad (5)$$

$$f(\mathbf{Q}, \mathbf{K}, \mathbf{V}) = \text{softmax} \left(\frac{\mathbf{Q} \mathbf{K}^T}{\sqrt{d_k}} \right) \times \mathbf{V}, \quad (6)$$

where \mathbf{Q} , \mathbf{K} , and \mathbf{V} denote the query, key, and value obtained from the feature maps, respectively. This method enables varying weights to be applied to the information provided by different nodes to each node in the graph. By assigning attention values to each node, data from various nodes can be combined to update the edge score, which helps to avoid duplication and loss of information. Additionally, the GDAN score matrix can be obtained directly from the network without changing its size. To generate the GDAN score matrix \mathbf{B} , a pre-learning phase is conducted using the self-attention block. The entry $B_{j,u}$ at the j -th row and u -th column of matrix \mathbf{B} is

$$B_{j,u} = \text{MLP}(\text{Attention}(\mathbf{Q}, \mathbf{K}, \mathbf{V}, \mathbf{B}_{init})). \quad (7)$$

The corresponding loss function for training the network to generate GDAN score matrix \mathbf{B} , association matrix loss, is expressed mathematically as

$$L_a = \sum_j^J \sum_u^U -y_{j,u} \log B_{j,u} - (1 - y_{j,u}) \log (1 - B_{j,u}). \quad (8)$$

This formula represents a cross-entropy loss that measures the difference between the predicted association scores ($B_{j,u}$) and the ground truth of the matching pair ($y_{j,u}$). Beware $y_{j,u}$ is a binary indicator which is either 0 or 1 as it represents the ground truth of the match between the u -th predicted object and the j -th detected object. When there is a clear match, $y_{j,u}$ is assigned as 1, and 0 otherwise. Due to the absence of ground-truth annotations for each pair, we define a match

based on object identity continuity between time frames: a pair is considered as "matched" if the closest ground-truth box to the tracking box in the previous time frame and the closest ground-truth box to the detection box in the current time frame have the same index and their IoU with their closest ground-truth boxes are more than 0.7. The value of $B_{j,u}$ is obtained from the GDAN score matrix \mathbf{B} and ranges between 0 and 1.

F. Association Module

In 3D MOT, the data association module plays a crucial role in determining the correspondence between detected and predicted objects, to update the state of the objects. Most of the methods used in 3D MOT rely on the minimization of the geometry association cost matrix. This is done by evaluating the overlap or distance between the 3D bounding boxes of the predicted and detected objects, using the global nearest neighbor principle and typically the Hungarian algorithm [61]. Recently, [38] proposed to incorporate geometry, motion and appearance features from images to construct such association cost matrix. In our proposed approach, we follow the similar idea to define the geometry and motion cost matrix, but using GDAN score matrix \mathbf{B} to replace the appearance features. The details are discussed in the follow parts.

Same as [38], the combination of geometry and motion cost matrix is expressed by the mathematical formulation

$$\mathbf{A} = \mathbf{Ge} + \mathbf{Mo}, \quad (9)$$

where the matrix \mathbf{Ge} denotes a geometry similarity matrix. This \mathbf{Ge} matrix establishes the correlations between the detected state after the offset correction module, denoted as \mathbf{Y}_t^{cor} , and the predicted state $\mathbf{X}_{t|t-1}$, via:

$$\mathbf{Ge} = IoU(\mathbf{Y}_t^{cor}, \mathbf{X}_{t|t-1}) + CEN(\mathbf{Y}_t^{cor}, \mathbf{X}_{t|t-1}). \quad (10)$$

The IoU in Eq. (10) is the cost from 3D IoU, which can be computed as

$$IoU = \frac{VI(\mathbf{Y}_t^{cor}, \mathbf{X}_{t|t-1})}{VOL(\mathbf{Y}_t^{cor}) + VOL(\mathbf{X}_{t|t-1}) - VI(\mathbf{Y}_t^{cor})}, \quad (11)$$

where VOL is the volume calculated by w, h, l in the state and VI denotes the volume intersection. The CEN in Eq. (10) is the cost from the centroid (in 3D Cartesian coordinate) [38] which can be computed as

$$CEN(\mathbf{Y}_t^{cor}, \mathbf{X}_{t|t-1}) = MSE(\mathbf{p}, \hat{\mathbf{p}}), \quad (12)$$

where \mathbf{p} refers to the global coordinates (x_p, y_p, z_p) for detected state (after the offset correction module) \mathbf{Y}_t^{cor} and $\hat{\mathbf{p}}$ is the corresponding value of predicted state $\mathbf{X}_{t|t-1}$.

$$Mo_{u,j} = w_{ang} * (1 - \cos \langle \tilde{v}, \hat{v} \rangle) + w_{velo} * MSE(\tilde{v}, \hat{v}), \quad (13)$$

where, w_{ang} is the weight for angle difference, w_{velo} is the weight for velocity difference, whereas \tilde{v} and \hat{v} denote the velocities of the predicted object states and detected object states respectively.

However, the current approach for calculating matrix \mathbf{A} is limited to considering only the geometry and motion costs, neglecting the valuable information embedded in the 3D

features present within the 3D point cloud. To address this limitation, we propose the final association cost matrix \mathbf{C} , which incorporates the geometry and motion cost matrix \mathbf{A} and the GDAN score matrix \mathbf{B} , respectively. This amalgamation is achieved through a weighted linear combination of \mathbf{A} and \mathbf{B} :

$$\mathbf{C} = \mathbf{A} - w_B \mathbf{B}, \quad (14)$$

where w_B represents the weight assigned to the GDAN score matrix \mathbf{B} . Notably, the subtraction operation between matrix \mathbf{A} and \mathbf{B} in Eq. (14) is performed due to the score being determined as a negative cost. By incorporating the GDAN score matrix alongside the geometry and motion cost matrix, our proposed method enriches the data association process, allowing for a more comprehensive evaluation of 3D features. With the final association cost matrix \mathbf{C} , as input, the Hungarian algorithm is used to solve the 2D assignment problem, identifying the matched pairs and unmatched objects.

G. State Update Module

Upon acquiring the association map from the association module, the Kalman filter is utilized to update the state of the predicted state. The updated mean \mathbf{X}_t and covariance \mathbf{P}_t are computed through the following Kalman update equations:

$$\mathbf{X}_t = \mathbf{X}_{t|t-1} + \mathbf{K}_f (\mathbf{Y}_t - \mathbf{H} \mathbf{X}_{t|t-1}), \quad (15)$$

$$\mathbf{P}_t = \mathbf{P}_{t|t-1} - \mathbf{K}_f \mathbf{S} \mathbf{K}_f^T, \quad (16)$$

$$\mathbf{S} = \mathbf{H} \mathbf{P}_{t|t-1} \mathbf{H}^T + \mathbf{R}, \quad (17)$$

$$\mathbf{K}_f = \mathbf{P}_{t|t-1} \mathbf{H}^T (\mathbf{H} \mathbf{P}_{t|t-1} \mathbf{H}^T + \mathbf{R})^{-1}, \quad (18)$$

where \mathbf{H} denotes the observation matrix selecting out the positional component from the object state, and \mathbf{R} is the measurement noise covariance matrix.

H. Track Management Module

In addition to the matched predicted states and the detected states, we should also deal with unmatched detected states, which may arise in two different cases: 1) Objects naturally disappear from the field of vision, and 2) Objects are misdetected, possibly due to temporary occlusion by other objects or movement beyond the optimal range of the LiDAR sensor.

In order to distinguish between these two cases, a threshold N^t is introduced. When a predicted state fails to be associated with any detected object for more than N^t consecutive time frames, it is presumed to have naturally disappeared. In such an event, the predicted state is eliminated and is no longer tracked. Conversely, predicted states that do not meet the above criteria are retained on the presumption that the objects may have been momentarily missed by the detector and could reappear in subsequent time.

TABLE I

Comparison of the proposed method and other state-of-the-art LiDAR-only trackers on front view 2D MOT tracking results using KITTI car test dataset.

Method	Modality	HOTA(%) \uparrow	AssA(%) \uparrow	LocA(%) \uparrow	MOTA(%) \uparrow	MOTP(%) \uparrow	MT(%) \uparrow	IDS \downarrow	FRAG \downarrow
AB3DMOT (IEEE IROS 2020)* [15]	L	69.99	69.33	86.85	83.61	85.23	66.92	113	206
PC3T (IEEE T-ITS 2022)*# [38]	L	77.80	81.59	86.07	88.81	84.26	80.00	225	201
Batch3DMOT (IEEE RA-L 2022)* [21]	L	<i>N/A</i>	<i>N/A</i>	<i>N/A</i>	88.60	86.80	76.70	19	74
LEGO (Ours)*	L	78.05	79.22	88.08	88.97	86.92	80.92	286	71
CenterTube (IEEE T-MM 2023)*** [34]	L	71.25	69.24	86.85	86.97	85.19	78.46	191	344
PolarMOT (ECCV 2022)** [35]	L	75.16	76.95	87.12	85.08	85.63	80.92	462	599
LEGO (Ours)**	L	79.52	83.34	87.49	88.14	86.06	87.54	290	117
UG3DMOT (Arxiv 2023)**** [36]	L	78.60	82.28	87.84	87.98	86.56	79.08	30	360
LEGO (Ours)****	L	80.75	83.27	87.92	90.61	86.66	87.85	214	109

* The metrics are reported by using PointRCNN [9] as 3D object detector.

** The metrics are reported by using PointGNN [10] as 3D object detector.

*** The metrics are reported by using CenterPoint [11] as 3D object detector, which has much better detection performance than PointGNN in general.

**** The metrics are reported by using CasA [12] as 3D object detector.

Note: Since the reported metrics of PC3T are based on the trajectory refinement, which makes PC3T an offline smoother rather than online tracker like all others, thus actual performance of online tracking version of PC3T is lower.

TABLE II

Comparison of the proposed method and other state-of-the-art LiDAR and camera fusion-based trackers on front view 2D MOT tracking results using KITTI car test dataset.

Method	Modality	HOTA(%) \uparrow	AssA(%) \uparrow	LocA(%) \uparrow	MOTA(%) \uparrow	MOTP(%) \uparrow	MT(%) \uparrow	IDS \downarrow	FRAG \downarrow
JMODT (IEEE IROS 2021) [46]	C+L	70.73	68.76	86.95	85.35	85.37	77.39	350	693
DeepFusionMOT (IEEE RA-L 2022)* [48]	C+L	75.46	80.05	86.70	84.63	85.02	68.61	84	472
StrongFusionMOT (IEEE S-J 2022)* [49]	C+L	75.65	79.84	86.74	85.53	85.07	66.15	58	416
LEGO (Ours)*	L	78.05	79.22	88.08	88.97	86.92	80.92	286	71
IMSF MOT (IEEE T-ITS 2023) [44]	C+L	72.44	68.02	<i>N/A</i>	90.32	85.47	86.46	526	270
EagerMOT (IEEE ICRA 2021)** [45]	C+L	74.39	74.16	87.17	87.82	85.69	76.15	239	390
DualTracker (IEEE T-IV 2023)** [47]	C+L	74.24	<i>N/A</i>	<i>N/A</i>	88.05	85.6	80.77	148	<i>N/A</i>
HIDMOT (IEEE T-VT 2023)** [50]	C+L	75.90	77.22	<i>N/A</i>	<i>N/A</i>	<i>N/A</i>	<i>N/A</i>	<i>N/A</i>	<i>N/A</i>
MSA-MOT (Sensors 2022)** [51]	C+L	78.52	82.56	87.00	88.01	85.45	86.77	91	428
LEGO (Ours)**	L	79.52	83.34	87.49	88.14	86.06	87.54	290	117

* The metrics are reported by using PointRCNN [9] as 3D object detector.

** The metrics are reported by using PointGNN [10] as 3D object detector.

IV. EXPERIMENTS AND ANALYSIS

In this section, we will discuss the results of our experiment. We will begin by providing an overview of the dataset used, followed by a description of the implementation details. Next, we will present a thorough ablation study. Lastly, we will compare our results with that of the baseline models.

A. Dataset and Evaluation Metrics

The popular LiDAR-based 3D detection and tracking benchmark dataset is KITTI [62]. In this work, we use the KITTI dataset as many LiDAR-based MOT methods have been evaluated within this dataset. The efficacy of our proposed LEGO modular tracker is assessed through the Higher-Order Tracking Accuracy (HOTA), defined as

$$HOTA = \int_0^1 HOTA_\alpha d\alpha \approx \frac{1}{19} \sum_{\alpha} HOTA_\alpha, \quad (19)$$

$$HOTA_\alpha = \sqrt{\frac{\sum_c A(c)}{fn + fp + tp}}, \quad (20)$$

where fn , fp , and tp represent the number of false negatives, false positives, and true positives, respectively, and $A(c)$ is the data association score. In Eq. (19), $\alpha \in$

$(0.05, 0.1, \dots, 0.9, 0.95)$ is a particular localization threshold used to determine false negatives and positives. In addition to HOTA, various other evaluation metrics are employed including Association Accuracy (AssA), Localization Accuracy (LocA), Multiple Object Tracking Accuracy (MOTA), Multiple Objects Tracking Precision (MOTP), Mostly Tracked Trajectories (MT - indicating the proportion of ground-truth trajectories that are at least 80% covered by the tracking output), Mostly Lost Trajectories (ML - denoting the proportion of ground-truth trajectories that are at most 20% covered by the tracking output), the quantity of Identity Switches (IDS), and the number of instances a trajectory is Fragmented (FRAG). The MOTA is defined as

$$MOTA = 1 - \frac{\sum_t fn_t + fp_t + idst_t}{\sum_t gt_t}, \quad (21)$$

where fn_t , fp_t , $idst_t$, and gt_t represent the number of false negatives, false positives, ID switch, and ground truth at time t respectively. The MOTP is defined as

$$MOTP = \frac{\sum_t dist_t}{\sum_t c_t}, \quad (22)$$

where $dist_t$ represents the distance between detection and its corresponding ground truth, and c_t is the number of matched

TABLE III

3D MOT tracking results of the proposed method and other state-of-the-art trackers on KITTI car validation dataset, by following the evaluation protocol in [15].

Method	Modality	sAMOTA(%)	AMOTA(%) \uparrow	AMOTP(%) \uparrow	MOTA(%) \uparrow	MOTP(%) \uparrow	IDS \downarrow	FRAG \downarrow
AB3DMOT (IEEE IROS 2020)* [15]	L	93.28	45.43	77.41	86.24	78.43	0	15
ACK3DMOT (IEEE T-IV 2023)* [33]	L	<i>N/A</i>	<i>N/A</i>	<i>N/A</i>	88.73	86.81	8	68
GNN3DMOT (IEEE CVPR 2020)* [43]	C+L	93.68	45.27	78.10	84.70	79.03	0	10
LEGO (Ours)*	L	94.90	47.78	86.97	91.36	86.70	1	4
CenterTube (IEEE T-MM 2023)*** [34]	L	93.89	46.24	80.23	<i>N/A</i>	<i>N/A</i>	78	<i>N/A</i>
PolarMOT (ECCV 2022)** [35]	L	94.32	<i>N/A</i>	<i>N/A</i>	93.93	<i>N/A</i>	31	<i>N/A</i>
EagerMOT (IEEE ICRA 2021)** [45]	C+L	94.94	48.80	80.40	96.61	80.00	2	<i>N/A</i>
HIDMOT (IEEE T-VT 2023)** [50]	C+L	<i>N/A</i>	45.64	79.68	90.45	81.44	<i>N/A</i>	<i>N/A</i>
CAMO-MOT (IEEE T-ITS 2023)** [52]	C+L	95.20	48.04	81.48	<i>N/A</i>	<i>N/A</i>	<i>N/A</i>	<i>N/A</i>
LEGO (Ours)**	L	95.20	48.10	87.05	92.00	86.69	1	5

* The metrics are reported by using PointRCNN [9] as 3D object detector.

** The metrics are reported by using PointGNN [10] as 3D object detector.

*** The metrics are reported by using CenterPoint [11] as 3D object detector, which has much better detection performance than PointGNN in general.

pairs at time t . Considering that the evaluation metrics on the KITTI benchmark are predominantly oriented towards a 2D perspective, additional comprehensive metrics pertinent to a 3D viewpoint are also employed, such as the Average Multiple Object Tracking Accuracy (AMOTA) and the corresponding precision metric, the Average Multiple Object Tracking Precision (AMOTP). AMOTA is defined as

$$AMOTA = \frac{1}{L} \sum_r \left(1 - \frac{\sum_t fn_t^r + fp_t^r + ids_t^r}{\sum_t gt_t} \right), \quad (23)$$

where fn_t^r , fp_t^r , ids_t^r represent the number of false negatives, false positives, ID switch at a specific recall value r at time t , L is the number of recall values respectively and AMOTP is defined as

$$AMOTP = \frac{1}{L} \sum_r (1 - MOTP_r), \quad (24)$$

where $MOTP_r$ is the value of MOTP at a specific recall r .

B. Implementation Details

During the training procedure, Adam with a momentum set as 0.09 and an initial learning rate of 0.1 is applied. The learning rate decay is 0.001, and the training is executed across 100 epochs. During the inference phase, the LiDAR scanning frequency is fixed at 10Hz, and the threshold for the existence probability provided by the object detector is set to 0. This means that all the objects provided by the object detector are kept as input to the tracker. Implementation details of the key modules are as follows:

Offset correction module: The kernel size, stride, and padding of the CNN layer are set to (3, 1, 1), respectively. The sizes of the two-layer MLP are set to (64, 6).

Feature extraction module: This module commences by setting the convolution channels to [64, 128, 1024] and configuring the kernel size and stride as 3 and 1, respectively, within the T-Net. Subsequently, a three-layer MLP is structured with sizes of (1024, 256, 128).

GDAN score calculation module: This module is characterized by setting the number of heads in each attention structure to 3, and GLUE is employed as the activation function.

The association self-attention block incorporates softmax as the normalization function for the adjacency matrix.

C. Performance Comparison with Other State-of-the-Arts

In this sub-section, the framework is evaluated and discussed with reference to a variety of MOT metrics.

1) Quality of Detection Input: The performance of a tracker is inherently tied to the effectiveness of the integrated detector. In the conducted experiments, three distinct object detectors were assessed: the CasA detector, the PointGNN detector, and the PointRCNN detector. These detectors were chosen based on their performance in the KITTI 3D Object detection challenge and arranged in descending order of effectiveness. As depicted in Table I, the tracking performances align with the quality of the detection input for all the assessed trackers. The result of our LEGO has been visualized in Fig. 6. The first row and the second show the ground truth and tracking result reported by our LEGO in scene 0006, the detected state in the current frame is marked by a bounding box and its track ID. The third row and the fourth-row show results in scene 0008.

2) Performance Comparison with State-of-the-Art Trackers Using LiDAR Only: As delineated in Table I, a series of comparative analyses were conducted on various tracking methodologies within the context of the KITTI tracking benchmark. First, we compare our method with PC3T [38], utilizing PointRCNN as the object detector. The results reveal that our method achieved an enhancement of 0.25 in HOTA and 0.37 in MOTA on the testing dataset. Further analysis is extended to other methodologies utilizing disparate detectors, as outlined in Table I. For instance, in a comparison with CenterTube [34], which employs the same detector PointGNN, our method demonstrate an improvement of 8.32 in HOTA and 1.17 in MOTA. Likewise, when compared with UG3DMOT [36] that utilizes the CasA detector, our method achieved an enhancement of 2.15 in HOTA and 2.63 in MOTA.

3) Performance Comparison with State-of-the-Art Trackers Using LiDAR and Camera: Many tracking algorithms leverage the fusion of 2D camera images and 3D point clouds to optimize performance within the KITTI tracking benchmark. Our

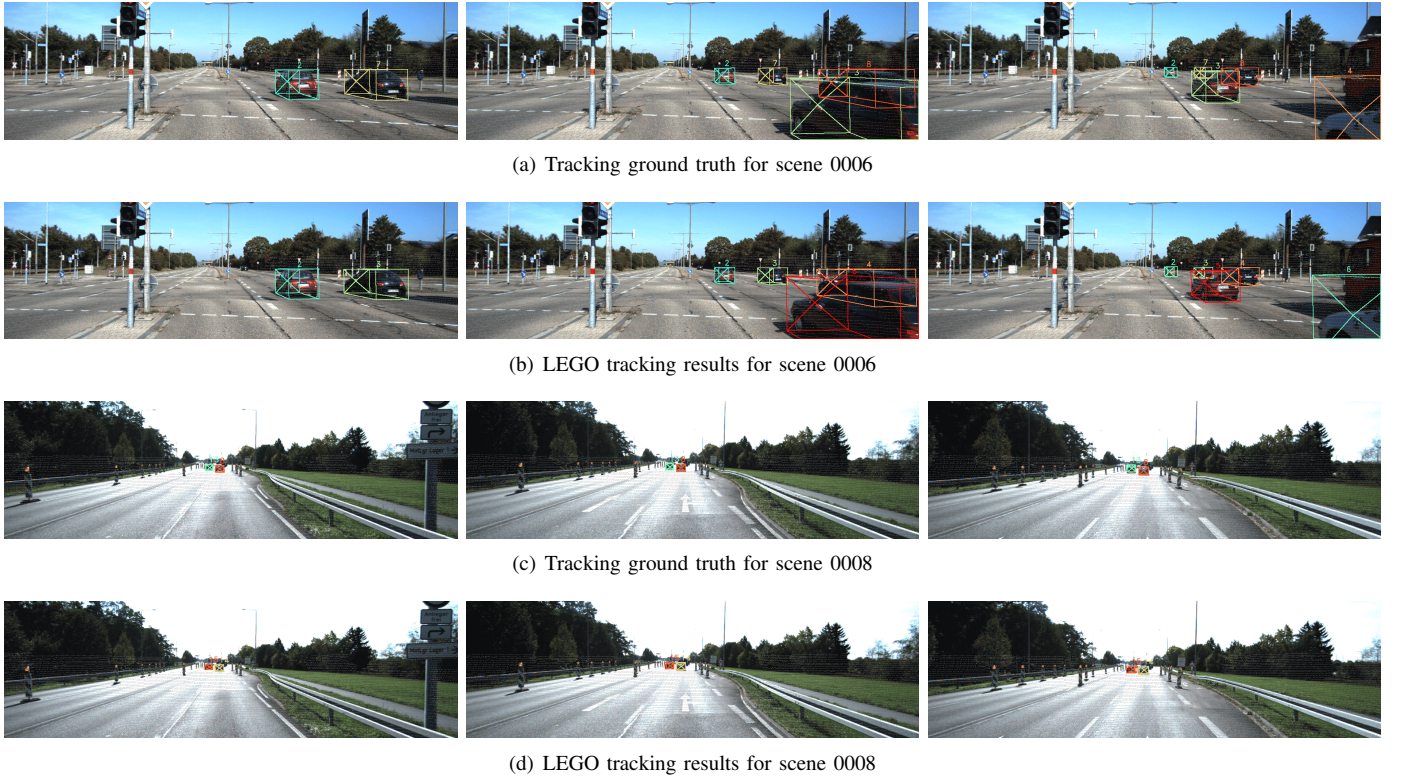


Fig. 6: This represents a demonstration of 3D MOT results utilizing the KITTI benchmark. The first and second rows display the tracking ground truth values and our proprietary LEGO model results, specifically within scene 0006. Within this context, the detected state (after the offset correction module) in the current frame is signified by the presence of a bounding box and an associated tracking identification number. The same objects have bounding boxes in the same colour with the same identification number. Similarly, the third and fourth rows offer an exhibition of the ground truth and employ our LEGO model results, albeit within a different context, scene 0008. These rows continue to utilize the detected state (after the offset correction module), marked by a bounding box and the tracking identification, to illuminate tracking methods within this unique environment.

proposed method, LEGO, was rigorously evaluated against a variety of LiDAR and camera fusion-based trackers. The comparative analysis was performed in two key segments in Table II, based on the detectors employed. Firstly, LEGO was compared with trackers utilizing PointRCNN as their detector. In this context, a notable improvement was observed against StrongFusionMOT [49], with LEGO registering 2.4 increments in HOTA and 3.44 increments in MOTA. The second segment of the comparative analysis involved trackers that employ PointGNN as their detector. LEGO's improvements were again manifest, with a 3.62 enhancement in HOTA over HIDMOT [50] and a 5.34 advancement in HOTA and 0.09 advancement in MOTA over DualTracker [47]. A specific comparison with IMSF-MOT [44] highlighted LEGO's superior performance.

4) *Comparison of Proposed Method and Other State-of-the-Art Trackers on 3D MOT Metrics:* Our proposed LEGO tracker has been subjected to extensive comparative evaluation against various trackers, employing front-view 3D MOT metrics, such as sAMOTA, AMOTA, and AMOTP. The details of these comparisons are tabulated in Table III. Against GNN3DMOT [43], LEGO demonstrated marked improvement across several fronts, with enhancements of 1.22 in sAMOTA, 2.51 in AMOTA, and 8.87 in AMOTP. The comparisons were further extended to trackers utilizing PointGNN as their

detector. When juxtaposed with CAMO-MOT [43], LEGO matched the SAMOTA, but exhibited improvement in AMOTA and AMOTP, by 0.06 and 5.57, respectively. Additionally, LEGO was evaluated against CenterTube, which utilizes CenterPoint as its detector, a system generally considered to offer superior detection performance over PointGNN. Nevertheless, as elucidated in Table III, despite using PointGNN as the detector, LEGO managed to secure improvements of 1.31 in sAMOTA, 1.86 in AMOTA, and 6.82 in AMOTP.

D. Ablation Study for LEGO Modular Tracker

This section outlines the process of parameter-tuning for LEGO, the car class type is taken as an example.

1) *Effectiveness of Weight between Matrix \mathbf{A} and Matrix \mathbf{B} :* Throughout the experimental phase, refinements were introduced to the cost weight w_B to ascertain the optimal equilibrium between the geometry and motion cost matrix \mathbf{A} , and the GDAN score matrix \mathbf{B} . A comprehensive assessment was conducted across four distinct levels for w_B , specifically 0, 1, 2, 3, and 4, as described in Table IV. It was found that when w_B was set to 2, the best outcomes were achieved. These results underscore the pivotal role played by the cost weight in determining the relative contributions of matrix \mathbf{A} and matrix \mathbf{B} to the association process.

TABLE IV

Ablation study on the weight w_B for matrix B with proposed method on KITTI car validation dataset.

w_B	HOTA(%)	AssA(%) \uparrow	LocA(%) \uparrow	MOTA(%) \uparrow
0	83.079	85.954	90.649	89.271
1	83.833	88.162	92.504	85.452
2	85.808	88.63	92.65	90.321
3	84.554	88.609	92.472	86.657
4	82.242	84.19	92.492	86.418

TABLE V

Ablation study on the threshold in track management with proposed method on KITTI car validation dataset.

N^t	HOTA(%)	AssA(%) \uparrow	LocA(%) \uparrow
10	85.305	86.704	92.371
12	85.522	87.045	92.35
14	85.808	88.63	92.65
15	84.411	88.452	92.469
24	84.189	88.198	92.457
34	83.692	87.466	92.337

2) *Effectiveness of Threshold in Track Management:* In the experiments, the N^t parameter was adjusted as 14 to manage tracks. Table V provides the results obtained by varying the threshold. These findings indicate that an optimal threshold pre-processing operation, combined with the appropriate cost weight used in the proposed LEGO tracker, can improve the HOTA score.

V. CONCLUSION

In this paper, we propose an online tracker, LEGO, that effectively integrates the geometry and motion cost matrix and GDAN score matrix to tackle the inherent challenges of MOT. The proposed tracker leverages 3D point cloud information, topological structures, and motion prediction features to enhance tracking accuracy and robustness. The incorporation of message passing and attention mechanisms within the GDAN enables efficient estimation of future motion states and the effective utilization of 3D point cloud data. Furthermore, our offset correction module demonstrates the capability to rectify certain errors in the detection results, contributing to improved tracking performance. However, it is important to acknowledge that the use of graph structures in our approach may lead to longer training times due to increased computational demands. As a potential solution for future research, techniques, such as voxel downsampling could be implemented to reduce the parameter count in the GNN, thereby enhancing computational efficiency and reducing time consumption.

REFERENCES

- J. Liu, W. Xiong, L. Bai, Y. Xia, T. Huang, W. Ouyang, and B. Zhu, “Deep instance segmentation with automotive radar detection points,” *IEEE Transactions on Intelligent Vehicles*, vol. 8, no. 1, pp. 84–94, 2023.
- W. Xiong, J. Liu, Y. Xia, T. Huang, B. Zhu, and W. Xiang, “Contrastive learning for automotive mmWave radar detection points based instance segmentation,” in *Proceedings of the IEEE International Conference on Intelligent Transportation Systems (ITSC)*, 2022, pp. 1255–1261.
- Y. Yang, J. Liu, T. Huang, Q.-L. Han, G. Ma, and B. Zhu, “RaLiBEV: Radar and LiDAR BEV fusion learning for anchor box free object detection systems,” 2022, *arXiv:2211.06108*, submitted to *IEEE Transactions on Neural Networks and Learning Systems*.
- J. Liu, Q. Zhao, W. Xiong, T. Huang, Q.-L. Han, and B. Zhu, “SMURF: Spatial multi-representation fusion for 3D object detection with 4D imaging radar,” *IEEE Transactions on Intelligent Vehicles*, Oct. 2023, doi: 10.1109/TIV.2023.3322729.
- W. Xiong, J. Liu, T. Huang, Q.-L. Han, Y. Xia, and B. Zhu, “LXL: LiDAR excluded lean 3D object detection with 4D imaging radar and camera fusion,” *IEEE Transactions on Intelligent Vehicles*, Oct. 2023, doi: 10.1109/TIV.2023.3321240.
- Y. Zhang, C. Wang, X. Wang, W. Zeng, and W. Liu, “FairMOT: On the fairness of detection and re-identification in multiple object tracking,” *International Journal of Computer Vision*, vol. 129, no. 11, pp. 3069–3087, Nov. 2021.
- Y. Zhang, P. Sun, Y. Jiang, D. Yu, Z. Yuan, P. Luo, W. Liu, and X. Wang, “Bytetrack: Multi-object tracking by associating every detection box,” in *Proceedings of the European Conference on Computer Vision (ECCV)*, 2022, pp. 1–21.
- Y. Du, Z. Zhao, Y. Song, Y. Zhao, F. Su, T. Gong, and H. Meng, “Strong-Sort: Make deepsort great again,” *IEEE Transactions on Multimedia*, 2023, doi: 10.1109/TMM.2023.3240881.
- S. Shi, X. Wang, and H. P. Li, “3D object proposal generation and detection from point cloud,” in *Proceedings of the IEEE/CVF Conference on Computer Vision and Pattern Recognition (CVPR)*, 2019, pp. 16–20.
- W. Shi, and R. Rajkumar, “Point-GNN: Graph neural network for 3D object detection in a point cloud,” in *Proceedings of the IEEE/CVF Conference on Computer Vision and Pattern Recognition (CVPR)*, 2020, pp. 1711–1719.
- T. Yin, X. Zhou, and P. Krahenbuhl, “Center-based 3D object detection and tracking,” in *Proceedings of the IEEE/CVF Conference on Computer Vision and Pattern Recognition (CVPR)*, 2021, pp. 11784–11793.
- H. Wu, J. Deng, C. Wen, X. Li, C. Wang, and J. Li, “CasA: A cascade attention network for 3D object detection from LiDAR point clouds,” *IEEE Transactions on Geoscience and Remote Sensing*, vol. 60, pp. 1–11, 2022.
- T. Gao, H. Pan, Z. Wang and H. Gao, “A CRF-based framework for tracklet inactivation in online multi-Object tracking,” *IEEE Transactions on Multimedia*, vol. 24, pp. 995–1007, 2022, doi: 10.1109/TMM.2021.3062489.
- W. Feng, L. Bai, Y. Yao, W. Gan, W. Wu and W. Ouyang, “Similarity-and quality-guided relation learning for joint detection and tracking,” *IEEE Transactions on Multimedia*, doi: 10.1109/TMM.2023.3279670.
- X. Weng, J. Wang, D. Held, and K. Kitani, “3D multi-object tracking: A baseline and new evaluation metrics,” in *Proceedings of the IEEE/RSJ International Conference on Intelligent Robots and Systems (IROS)*, 2020, pp. 10359–10366.
- S. Särkkä, and L. Svensson, “Bayesian filtering and smoothing,” *Cambridge university press*, vol. 17, 2023.
- H.-K. Chiu, A. Prioletti, J. Li, and J. Bohg, “Probabilistic 3D multi-object tracking for autonomous driving,” 2020, *arXiv:2001.05673*.
- S. Pang, D. Morris, and H. Radha, “3D multi-object tracking using random finite set-based multiple measurement models filtering (RFS-M3) for autonomous vehicles,” in *Proceedings of the IEEE International Conference on Robotics and Automation (ICRA)*, 2021, pp. 13701–13707.
- C. Luo, X. Yang, and A. Yuille, “Exploring simple 3D multi-object tracking for autonomous driving,” in *Proceedings of the IEEE/CVF International Conference on Computer Vision (ICCV)*, 2021, pp. 10488–10497.
- J.-N. Zaech, A. Liniger, D. Dai, M. Danelljan, and L. Van Gool, “Learnable online graph representations for 3D multi-object tracking,” *IEEE Robotics and Automation Letters*, vol. 7, no. 2, pp. 5103–5110, 2022.
- M. Büchner, and A. Valada, “3D multi-object tracking using graph neural networks with cross-edge modality attention,” *IEEE Robotics and Automation Letters*, vol. 7, no. 4, pp. 9707–9714, 2022.
- Z. Pang, Z. Li, and N. Wang, “SimpleTrack: Understanding and re-thinking 3D multi-object tracking,” in *Proceedings of the European Conference on Computer Vision (ECCV) Workshop*, 2022, pp. 680–696.
- Q. Wang, Y. Chen, Z. Pang, N. Wang, and Z. Zhang, “Immortal tracker: Tracklet never dies,” 2021, *arXiv:2111.13672*.
- F. Meyer, T. Kropfreiter, J. L. Williams, R. Lau, F. Hlawatsch, P. Braca, and M. Z. Win, “Message passing algorithms for scalable multitarget tracking,” in *Proceedings of the IEEE*, vol. 106, no. 2, pp. 221–259, Feb. 2018.
- F. Ruppel, F. Faion, C. Gläser, and K. Dietmayer, “Transformers for multi-object tracking on point clouds,” in *Proceedings of the IEEE Intelligent Vehicles Symposium (IV)*, 2022, pp. 832–838.
- T. Wen, Y. Zhang, and N. M. Freris, “PF-MOT: Probability fusion based

3D multi-object tracking for autonomous vehicles," in *Proceedings of the International Conference on Robotics and Automation (ICRA)*, 2022, pp. 700-706.

[27] M. Liang and F. Meyer, "Neural enhanced belief propagation for multiobject tracking," *IEEE Transactions on Signal Processing*, 2023, doi: 10.1109/TSP.2023.3314275.

[28] J. Liu, L. Bai, Y. Xia, T. Huang, B. Zhu, and Q. -L. Han, "GNN-PMB: A simple but effective online 3D multi-object tracker without bells and whistles," *IEEE Transactions on Intelligent Vehicles*, vol. 8, no. 2, pp. 1176-1189, 2023.

[29] J. Willes, C. Reading, and S. L. Waslander, "Intertrack: Interaction transformer for 3D multi-object tracking," 2022, *arXiv:2208.08041*.

[30] J. Gwak, S. Savarese and J. Bohg, "Minkowski tracker: A sparse spatio-temporal R-CNN for joint object detection and tracking," 2022, *arXiv:2208.10056*.

[31] T. Sadjadpour, J. Li, R. Ambrus, and J. Bohg, "ShaSTA: Modeling shape and spatio-Temporal affinities for 3D multi-object tracking," 2022, *arXiv:2211.03919*.

[32] Y. Zhang, X. Wang, X. Ye, W. Zhang, J. Lu, X. Tan, E. Ding, P. Sun, and J. Wang, "ByteTrackV2: 2D and 3D multi-object tracking by associating every detection box," 2023, *arXiv:2303.15334*.

[33] G. Guo and S. Zhao, "3D multi-object tracking with adaptive cubature Kalman filter for autonomous driving," *IEEE Transactions on Intelligent Vehicles*, vol. 8, no. 1, pp. 84-94, 2023.

[34] H. Liu, Y. Ma, Q. Hu, and Y. Guo, "CenterTube: Tracking multiple 3D objects with 4D tubelets in dynamic point clouds," *IEEE Transactions on Multimedia*, Feb 2023, doi: 10.1109/TMM.2023.3241548.

[35] A. Kim, G. Brasó, A. Ošep, and L. Leal-Taixé, "PolarMOT: How far can geometric relations take us in 3D multi-object tracking?," in *Proceedings of the European Conference of Computer Vision (ECCV)*, 2022, pp. 41-58.

[36] J. He, C. Fu, and X. Wang, "3D multi-object tracking based on uncertainty-guided data association," 2023, *arXiv:2303.01786*.

[37] L. Wang, J. Zhang, P. Cai, and X. Li, "Towards robust reference system for autonomous driving: Rethinking 3D MOT," in *Proceedings of the IEEE International Conference on Robotics and Automation (ICRA)*, 2023, pp. 8319-8325.

[38] H. Wu, W. Han, C. Wen, X. Li, and C. Wang, "3D multi-object tracking in point clouds based on prediction confidence-guided data association," *IEEE Transactions on Intelligent Transportation Systems*, vol. 23, no. 6, pp. 5668-5677, 2022.

[39] H. Wu, Q. Li, C. Wen, X. Li, X. Fan, and C. Wang, "Tracklet proposal network for multi-object tracking on point clouds," in *Proceedings of the International Joint Conferences on Artificial Intelligence (IJCAI)*, 2021, pp. 1165-1171.

[40] H.-K. Chiu, J. Li, R. Ambruš, and J. Bohg, "Probabilistic 3D multi-modal, multi-object tracking for autonomous driving," in *Proceedings of the IEEE International Conference on Robotics and Automation (ICRA)*, 2021, pp. 14227-14233.

[41] N. Benbarka, J. Schröder, and A. Zell, "Score refinement for confidence-based 3D multi-object tracking," in *Proceedings of IEEE/RSJ International Conference on Intelligent Robots and Systems (IROS)*, 2021, pp. 8083-8090.

[42] Y. Zeng, C. Ma, M. Zhu, Z. Fan, and X. Yang, "Cross-modal 3D object detection and tracking for auto-driving," in *Proceedings of the 2021 IEEE/RSJ International Conference on Intelligent Robots and Systems (IROS)*, 2021, pp. 3850-3857.

[43] X. Weng, Y. Wang, Y. Man, and K. M. Kitani, "GNN3DMOT: Graph neural network for 3D multi-object tracking with 2D-3D multi-feature learning," in *Proceedings of the IEEE Conference on Computer Vision and Pattern Recognition (CVPR)*, 2020, pp. 6499-6508.

[44] G. Wang, C. Peng, Y. Gu, J. Zhang, and H. Wang, "Interactive multi-scale fusion of 2D and 3D features for multi-object vehicle tracking," *IEEE Transactions on Intelligent Transportation Systems*, May 2023, doi: 10.1109/TITS.2023.3275954.

[45] A. Kim, A. Ošep, and L. Leal-Taixé, "EagerMOT: 3D multi-object tracking via sensor fusion," in *Proceedings of the IEEE International Conference on Robotics and Automation (ICRA)*, 2021, pp. 11315-11321.

[46] K. Huang, and Q. Hao, "Joint multi-object detection and tracking with camera-LiDAR fusion for autonomous driving," in *Proceedings of the IEEE/RSJ International Conference on Intelligent Robots and Systems (IROS)*, 2021, pp. 6983-6989.

[47] Y. Ma, J. Zhang, G. Qin, J. Jin, K. Zhang, D. Pan, and M. Chen, "3D multi-object tracking based on dual-tracker and DS evidence theory," *IEEE Transactions on Intelligent Vehicles*, vol. 8, no. 3, pp. 2426-2436, 2023.

[48] X. Wang, C. Fu, Z. Li, Y. Lai and J. He, "DeepFusionMOT: A 3D multi-object tracking framework based on camera-LiDAR fusion with deep association," *IEEE Robotics and Automation Letters*, vol. 7, no. 3, pp. 8260-8267, 2022.

[49] X. Wang, C. Fu, J. He, S. Wang, and J. Wang, "StrongFusionMOT: A multi-object tracking method based on LiDAR-camera fusion," *IEEE Sensors Journal*, Dec 2022, doi: 10.1109/JSEN.2022.3226490.

[50] Y. An, J. Wu, Y. Cui, and H. Hu, "Multi-object tracking based on a novel feature image with multi-modal information," *IEEE Transactions on Vehicular Technology*, March 2023, doi: 10.1109/TVT.2023.3259999.

[51] Z. Zhu, J. Nie, H. Wu, Z. He, and M. Gao, "MSA-MOT: Multi-stage association for 3D multimodality multi-object tracking," *Sensors*, vol. 22, no. 22, pp. 8650, 2022.

[52] L. Wang, X. Zhang, W. Qin, X. Li, L. Yang, Z. Li, L. Zhu, H. Wang, and H. Liu, "CAMO-MOT: Combined appearance-motion optimization for 3D multi-object tracking with camera-LiDAR fusion," *IEEE Transactions on Intelligent Transportation Systems*, June 2023, doi: 10.1109/TITS.2023.3285651.

[53] Weng, X., Yuan, Y. and Kitani, K., "PTP: Parallelized tracking and prediction with graph neural networks and diversity sampling," *IEEE Robotics and Automation Letters*, 2021, pp.4640-4647.

[54] Ding, S., Rehder, E., Schneider, L., Cordts, M. and Gall, J. "3dmot-former: Graph transformer for online 3d multi-object tracking," in *Proceedings of the IEEE/CVF International Conference on Computer Vision*, 2023, pp. 9784-9794.

[55] C. H. Kuo, C. Huang, and R. Nevatia " Multi-target tracking by online learned discriminative appearance models", *IEEE Conference on Computer Vision and Pattern Recognition (CVPR)*, 2010, pp. 685-692.

[56] A. Alahi, K. Goel, V. Ramanathan, A. Robicquet, F.-F. Li, and S. Savarese, "Social LSTM: Human trajectory prediction in crowded spaces," in *Proceedings of the IEEE Conference on Computer Vision and Pattern Recognition*, 2016, pp. 961-971.

[57] H. N. Hu, Q.Z. Cai, D. Wang, J. Lin, M. Sun, P. Krahenbuhl, T. Darrell, and F. Yu, "Joint monocular 3D vehicle detection and tracking," *IEEE/CVF International Conference on Computer Vision*, 2019, pp. 5390-5399.

[58] C. R. Qi, H. Su, K. Mo, and L.J. Guibas, "Pointnet: Deep learning on point sets for 3D classification and segmentation." *IEEE Conference on Computer Vision and Pattern Recognition*, 2017, pp. 652-660.

[59] X. Jiang, P. Li, Y. Li, and X. Zhen, " Graph neural based end-to-end data association framework for online multiple-object tracking," 2019, *arXiv:1907.05315*.

[60] P. Veličković, G. Cucurull, A. Casanova, A. Romero, P. Lio and Y. Bengio, "Graph attention networks," 2017, *arXiv:1710.10903*.

[61] B. Samuel, and R. Popoli. "Design and analysis of modern tracking systems," *Artech House*, 1999.

[62] A. Geiger, L. Philip, S. Christoph, and U. Raquel, "Vision meets robotics: The KITTI dataset," *The International Journal of Robotics Research*, vol. 32, no. 11, pp. 1231-1237, Aug. 2013.